photonics

MDPI

Article

Collagen Organization, Polarization Sensitivity and Image Quality in Human Corneas using Second Harmonic Generation Microscopy

Juan M. Bueno [1,*], Rosa M. Martínez-Ojeda [1], Inés Yago [2] and Francisco J. Ávila [3]

[1] Laboratorio de Óptica, Instituto Universitario de Investigación en Óptica y Nanofísica, Universidad de Murcia, Campus de Espinardo (Ed. 34), 30100 Murcia, Spain
[2] Servicio de Oftalmología, Hospital Virgen de la Arrixaca, 30120 Murcia, Spain
[3] Department Física Aplicada, Universidad de Zaragoza, 50009 Zaragoza, Spain
* Correspondence: bueno@um.es

Abstract: In this paper, a Second-Harmonic-Generation (SHG) microscope was used to study the relationship between collagen structural arrangement, image quality and polarization sensitivity in human corneas with different organizations. The degree of order (or alternatively, the Structural Dispersion, SD) was quantified using the structure tensor method. SHG image quality was evaluated with different objective metrics. Dependence with polarization was quantified by means of a parameter defined as polarimetric modulation, which employs polarimetric SHG images acquired with four independent polarization states. There is a significant exponential relationship between the quality of the SHG images and the SD of the samples. Moreover, polarization sensitivity strongly depends on collagen arrangement. For quasi- or partially organized specimens, there is a polarization state that noticeably improves the image quality, providing additional information often not seen in other SHG images. This does not occur in non-organized samples. This fact is closely related to polarimetric modulation, which linearly decreases with the SD. Understanding in more detail the relationships that take place between collagen distribution, image quality and polarization sensitivity brings the potential to enable the development of optimized SHG image acquisition protocols and novel objective strategies for the analysis and detection of pathologies related to corneal collagen disorders, as well as surgery follow-ups.

Keywords: second harmonic generation; cornea imaging; polarization sensitivity

Citation: Bueno, J.M.; Martínez-Ojeda, R.M.; Yago, I.; Ávila, F.J. Collagen Organization, Polarization Sensitivity and Image Quality in Human Corneas using Second Harmonic Generation Microscopy. *Photonics* **2022**, *9*, 672. https://doi.org/10.3390/photonics9100672

Received: 20 July 2022
Accepted: 13 September 2022
Published: 20 September 2022

1. Introduction

The cornea is the outer transparent structure of the eye responsible for two-thirds of its focusing power. About 90% of the whole corneal thickness corresponds to the stroma, which is mainly composed of type I collagen fibers [1]. Since 2002, Second-Harmonic-Generation (SHG) microscopy has been widely used for label-free non-invasive imaging of the corneal stroma [2].

Although stromal fibers present different spatial distributions depending on the species, healthy corneas usually present quasi- or partially organized patterns [3–5]. It is believed that the transparency of the cornea relies on the special spatial distribution of the collagen within the stroma [6,7]; however, different arrangements have shown similar transparency [5].

SHG imaging of the cornea has attracted increasing attention from the biophotonics community, not only for the exploration of healthy samples but also for the analysis of changes associated with different pathologies [8]. The effects of surgical procedures and external damages have also been studied [9–11].

Despite a number of animal models (birds, rabbits, rats, bovines, etc.) being used, the extrapolation of results to human corneal tissues is not always straightforward since the

natural collagen distributions are not the same. Corneas from human donors are more difficult to obtain than those from animal models. Nevertheless, different authors have analyzed human corneal pathologies through SHG microscopy, including keratoconus, keratitis and bullous keratopathy, among others [12–14]. Other experiments were focused on the evaluation of corneas before transplantation [15,16] or after collagen cross-linking [17]. Changes suffered by human corneas under different experimental conditions were not always measured quantitatively. However, during recent years, different algorithms have been reported [8,15,17,18].

In addition, the visualization of the corneal stroma is challenging in clinical environments. To date, SHG microscopy is the only technique able to provide images of collagen fibers at micrometric resolution, even in living human eyes [19]. Objective assessments of corneal abnormalities are directly related to the presence of certain pathologies [18], even before the patient is aware of them. Alterations in the corneal organization might seriously compromise functional and optical functions, but they are not always readily visible. However, accurate medical diagnoses based on observations require images of enough quality and visible features to differentiate pathological stages. To the best of our knowledge, an analysis of the image quality from early to late human corneal pathological stages is lacking in the literature.

Moreover, SHG signals are sensitive to the polarization configuration as earlier reported by Roth and Freund in 1979 [20]. This property extends the potential of SHG imaging and can be used to extract information related to the collagen structure [21,22]. The relationship between SHG emissions and the alignment between collagen fibers has been reported in different collagen-based tissues, but experiments involving ocular tissues (the cornea in particular) are scarce [10,23–25]. Since SHG images acquired under different incident polarization states exhibit distinct characteristics in terms of content and appearance [26], the visualization of special details might be optimized and highlighted using certain polarization states, which might be of special importance in diseased corneas. The authors have not found previous studies reporting how polarization sensitivity and collagen spatial distribution are related to each other in human corneas.

In this study, we investigated the relationship between collagen arrangement, image quality and polarization sensitivity in human corneas with different degrees of organization, as measured with the structure tensor method [27].

2. Materials and Methods

2.1. Experimental Setup

Measurements were performed using a custom SHG microscope (Figure 1). This setup consists of an 800 nm femtosecond laser (Mira900; Coherent, Santa Clara, CA), an inverted microscope (Nikon TE2000-U; Nikon Corporation, Tokyo, Japan), a galvanometric scanner (XY unit) and a long-working-distance 40× NA 0.5 non-immersion objective (OBJ, Nikon ELWD Series; Nikon Corporation, Tokyo, Japan). A telescopic system (not shown) conjugates the XY unit and the entrance pupil of the OBJ.

A polarization state generator (PSG) was placed in the illumination pathway. This PSG, composed of a fixed horizontal linear polarizer and a set of $\lambda/2$ + $\lambda/4$ waveplates, was used to produce four independent polarization states named as PS1, PS2, PS3 and PS4. Differences in power at the sample's plane for each PS polarization were <2%. A neutral density filter (NDF) was used to control the laser power reaching the cornea. Further details on how these PSs were produced, and extra technical details about the instrument can be found in [28].

SHG signals from the samples were detected in a backward direction, using a photomultiplier tube (PMT, R7205-01; Hamamatsu, Shizouka, Japan). A narrow band spectral filter (400 ± 10 nm) placed in front of the PMT was used to isolate the SHG signal. SHG images were acquired at 1 Hz, and they had a size of 180 × 180 μm^2 (250 × 250 pixels). The system was fully controlled through home-made LabVIEW^{TM} software (LabVIEW

2009; National Instruments, Austin, TX, USA). Image processing was performed using MatLab^{TM} (MatLab 2017a; MathWorks Inc, Natick, MA, USA).

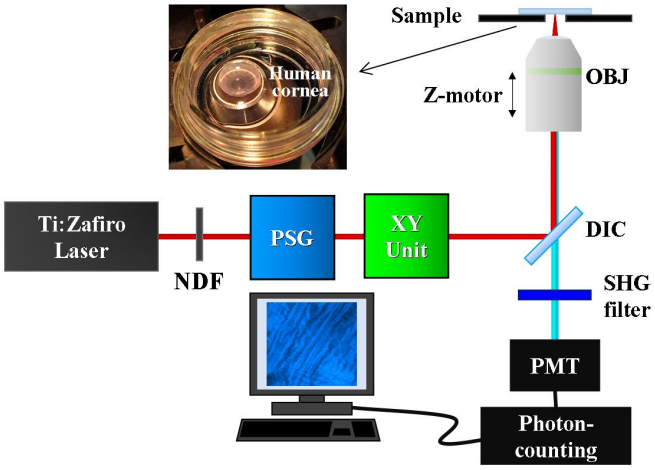

Figure 1. Sketch of the SHG microscope used for imaging human corneas. NDF, neutral density filter; PSG, polarization state generator; DIC, dichroic mirror; OBJ, objective; PMT, photo-multiplier tube. The inset corresponds to a specimen ready to be imaged.

2.2. Imaging Procedure and Analysis

The experiment was divided into two parts. For the first part, the PSG was set to produce circular polarized light (PS1). The total intensity of each acquired SHG image was computed, as well as different image quality parameters, such as acutance and entropy [29,30]. When required, intensity profiles were also calculated to compare local sharpness and features within the images.

In addition, the information on the collagen arrangement of the corneal stroma was objectively computed through the structure tensor procedure. A detailed description of this mathematical tool can be found in [27]. This algorithm provides different quantitative parameters related to the degree of organization of a spatially resolved structure. An illustrative example is depicted in Figure 2. In particular, the histogram of preferential orientations (POs) and the Structural Dispersion (SD) were used in this work. In general terms, a high (low) SD is associated with low (high) organization of the collagen-based sample. More specifically, if SD $\leq 20°$, the SHG images present fibers mostly aligned along a certain PO (i.e., the PO histogram shows a well-defined peak), and the sample presents a quasi-aligned distribution. When $20° < SD < 40°$, the distribution is considered as partially organized (i.e., the histogram broadens). For SD values higher than 40°, a non-organized structure is present, and a PO does not appear in the PO histogram.

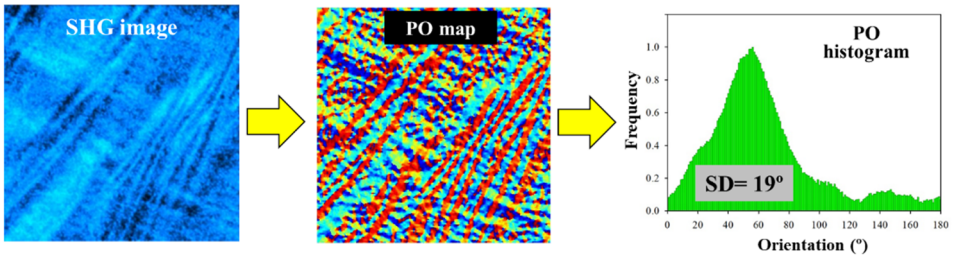

Figure 2. A schematic diagram that shows the use of the structure tensor. SHG images to be processed (**left panel**); spatially resolved map of POs (**central panel**); PO histogram showing the frequency of appearance of a certain orientation of the fibers within the SHG image (**right panel**). The value of SD is also presented for clarity (this is defined as the standard deviation of the PO histogram).

For the second part of the experiment, four SHG images corresponding to the predefined PSs (PS1–PS4) were recorded for each sample involved in the study. For each set of four images, the map of polarimetric modulation was computed (pixel-by-pixel) using the following equation:

$$Modulation(x,y) = \frac{I^{max}_{[PS1-PS4]}(x,y) - I^{min}_{[PS1-PS4]}(x,y)}{I^{max}_{[PS1-PS4]}(x,y) + I^{min}_{[PS1-PS4]}(x,y)}, \quad (1)$$

where, for each pixel (x, y), $I^{max}_{[PS1-PS4]}$ ($I^{min}_{[PS1-PS4]}$) is the maximum (minimum) intensity of the set of the four SHG images [PS1, PS2, PS3, PS4]. The relationship between this polarimetric modulation and the SD was analyzed.

These maps provide information on the spatially resolved polarization sensitivity of the samples. Then, local information can be obtained and particular features highlighted. Since this parameter ranges between 0 and 1, the closer to 0 (1), the lower (higher) the polarization dependence. That is, if the modulation is close to zero, there is hardly any dependence between the SHG intensity and the incoming polarization state.

2.3. Samples

Human corneas (N = 13) were provided by the eye bank of the Hospital Universitario Virgen de la Arrixaca, Murcia, Spain. Healthy specimens used in this study were not suitable for transplantation due to a variety of reasons (N = 8). Pathological samples were obtained from patients suffering from different pathologies, such as keratoconus, leucoma, pellucid marginal degeneration and corneal ulcers. The entire study was approved by the Ethical Review Board of both the Universidad de Murcia and the Hospital. All samples were treated following the tenets of the Declaration of Helsinki.

Since these pathologies were already at an advanced stage (patients underwent different types of keratoplasty), a model of pathology progression was planned to analyze the evolution of the structure-related parameters studied here. This was based on a temporal edema generated by overhydration [31]. A (healthy) cornea was immersed in a PBS solution for 24 h to induce edema. SHG images were acquired at five different time points (0–4). The edematous cornea imaged at time points 1, 2, 3 and 4 is treated as different samples (this means that the total number of individual samples in the following plot is 17). All SHG images used here corresponded to the anterior corneal stroma.

3. Results

3.1. Structural Dispersion and Image Quality

Shown in Figure 3 (upper panels) is a representative example of three SHG images of the human stroma corresponding to the different sets of collagen organization described above (see SD values in the insets as a reference). Figure 3a,b correspond to two healthy corneas (apex and peripheral area, respectively), and Figure 3c corresponds to a pathological one (keratoconus). Qualitative differences among the images can be easily observed. The morphological alterations present in the sample of Figure 3c are a result of the pathological process.

For all samples involved in this study, the SD was computed through the structure tensor protocol as indicated in the Materials and Methods. This analysis was used to quantitatively assess alterations in the organization of collagen fibers. Figure 3d–f depict the histograms of the POs for the SHG images presented in the upper row of Figure 3. As expected, the collagen distribution of the healthy specimens (organized and partially aligned arrangement, SD < 40°) presents POs associated with the peak of the histograms. Contrastingly, the keratoconus cornea exhibits a non-organized structure (i.e., SD > 40°) and an absence of PO.

The SD values were computed for all samples involved in the experiment. The minimum and maximum values were 17° and 52°, respectively, for the set of human

corneal tissues used. According to these results, the samples were distributed as follows: N = 3 (quasi-organized), N = 9 (partially organized) and N = 5 (non-organized).

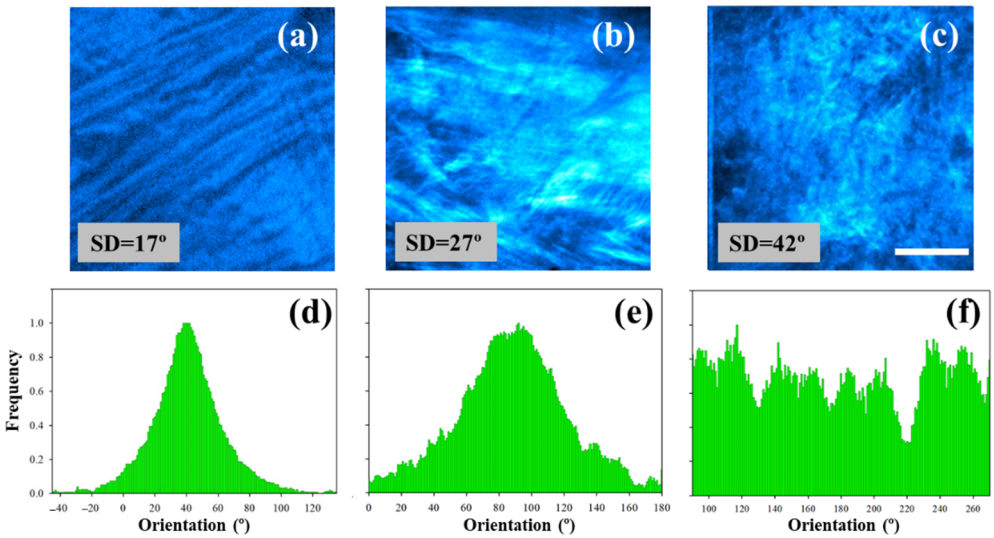

Figure 3. SHG images of non-pathological human corneas (**a**,**b**) and a cornea affected by keratoconus (**c**). Scale bar = 50 µm. (**d**–**f**) Histograms of PO distribution for the SHG images of the upper row. These were calculated using the structure tensor.

The SHG images corresponding to the samples used as a temporal model for edema are shown in Figure 4. Changes in collagen organization are readily visible when comparing images from left to right. Progressive collagen denaturation takes place as the amount of edema increases, which is associated with an increase in SD (Figure 5a). In addition, the loss of fiber delineation produced by the presence of the edema can be quantified via the intensity profiles along the black dotted line depicted in Figure 4a. The effect is shown in Figure 5b.

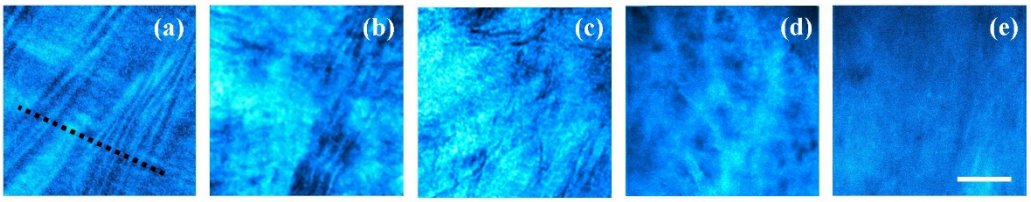

Figure 4. SHG images corresponding to the temporal evolution of a human corneal edema. (**a**) Control cornea (time point 0); (**b**–**d**) edema progression (time points 1–3); (**e**) final severe edematous cornea (i.e., opaque tissue, time point 4). Bar length = 50 µm.

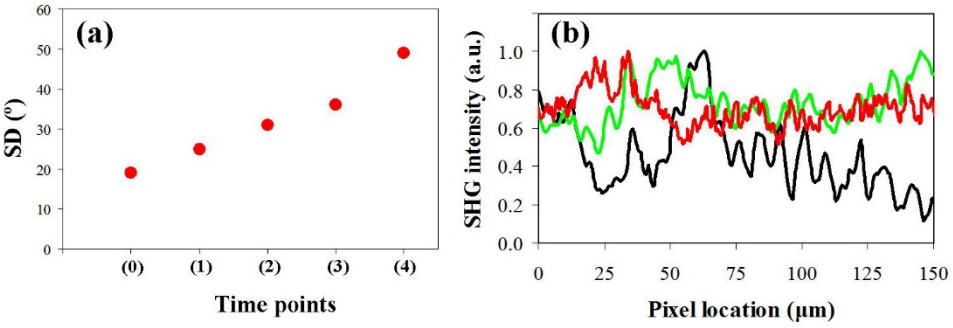

Figure 5. (**a**) Human edema temporal progression in terms of SD. (**b**) Intensity profiles for SHG images in Figure 4, along the indicated dotted line. Black line: control (Figure 4a); green and red lines: two different temporal stages (Figure 4c,e, respectively).

As seen above, the increase in SD within the corneal stroma is closely related to the presence of certain pathologies. In clinical environments, the visualization and analysis of these changes in the collagen arrangement are of relevant importance. Consequently, it is interesting to determine whether the quality of these images is associated with the collagen organization. In relation to this, Figure 6 shows the values of acutance of each SHG image as a function of SD. A significant exponential decay was found for this image quality parameter (R = 0.96, $p < 0.0001$).

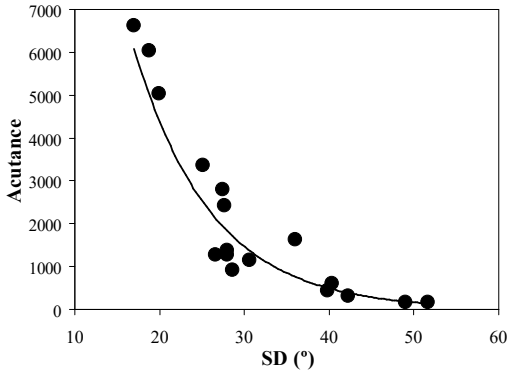

Figure 6. Acutance vs. SD values for all SHG images involved in the present experiment.

For the sense of completeness, Figure 7 presents the values of entropy also as a function of the SD of each samples. Similar to what occurs with acutance, the entropy was also strongly correlated with SD. This image quality metric also follows an exponential decrease (R = 0.91, $p < 0.0001$). However, the decay is not as abrupt as that found for acutance.

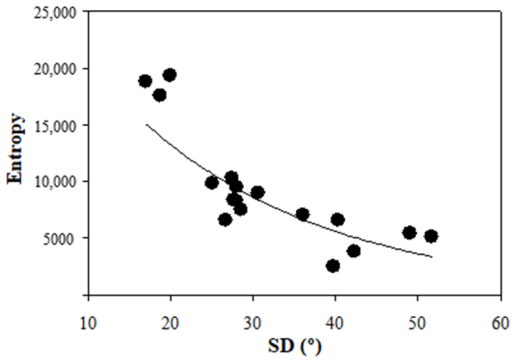

Figure 7. Entropy values as a function of SD for all images considered herein.

3.2. Structural Dispersion and Polarimetric Modulation

For every sample used in this study, four polarimetric SHG images were acquired, each corresponding to an independent PS produced by the PSG (see Methods). Figure 8 presents examples of these SHG images for two samples with different SD values.

In order to examine the differences among images within a set, the total SHG intensity was computed. For these two particular cases, the results are given in Figure 9. For images in the upper panel, the difference between the maximum and minimum intensity was 77% (blue symbols), whereas for the images in the lower panel, this was 31% (green symbols).

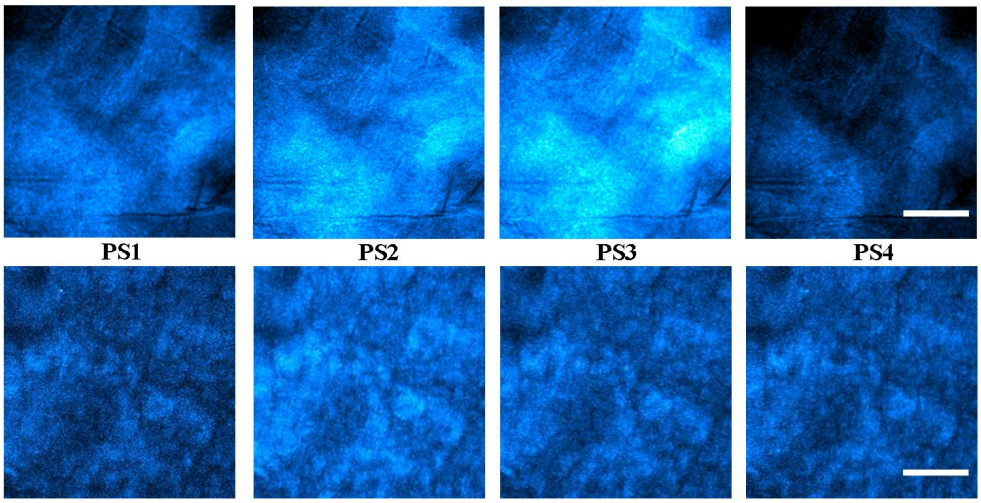

Figure 8. SHG images acquired for 4 independent polarization states (as indicated) for samples with SD = 27° (upper panels) and 40° (bottom panels). Bar length: 50 μm.

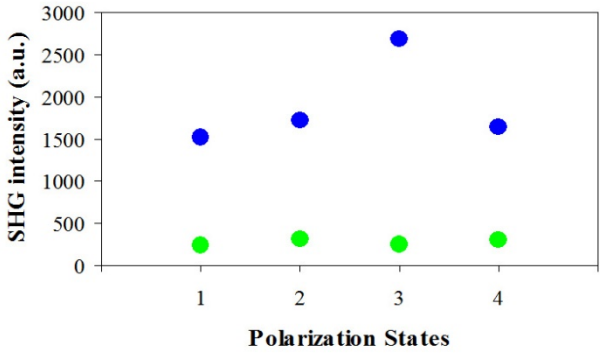

Figure 9. SHG intensity values for the SHG images of the precedent figure (blue, upper panels; green, bottom panels).

For a better analysis of these differences, Figure 10 shows the maps resulting from computing the pixel-by-pixel polarimetric modulation (see Equation (1) in Section 2.2) across the entire images. As expected, Figure 9 shows the modulation for the sample with a lower SD, which presents a color hotter than that corresponding to the specimen with a higher SD. Notably, the SD provides a global assessment of the collagen distribution, whereas the maps of modulation add extra information on local variations of this arrangement across the SHG image.

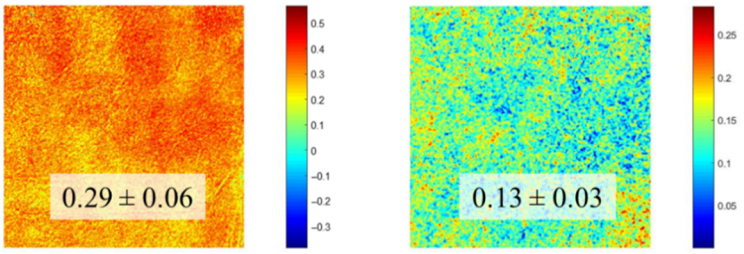

Figure 10. Spatially resolved maps of polarimetric modulation computed from the SHG images in Figure 8. The values in the insets are the averaged values across each map, with the corresponding standard deviation.

In order to gain more insight into this effect, Figure 11 depicts the values of polarimetric modulation of the SHG images (averages across the entire maps) as a function of SD. A

decreasing linear significant correlation is present (R = 0.84, $p < 0.0001$; best linear fit: Mod = −0.009·SD + 0.52). This means that the higher the collagen organization, the higher the modulation (or alternatively, the sensitivity to polarization).

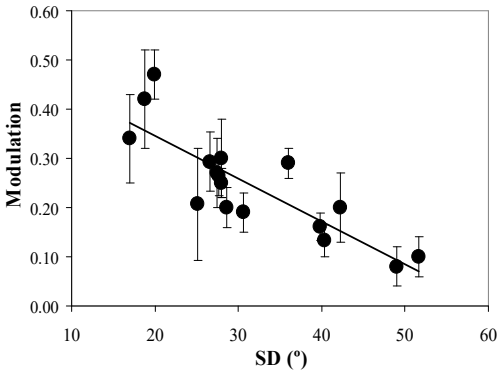

Figure 11. Polarimetric modulation vs. SD for all images involved in the present experiment. Each symbol is the average values across the entire map. Bars represent the standard deviation.

4. Discussion

For almost two decades, SHG microscopy has emerged as a powerful imaging tool to discriminate pathological tissues from healthy tissues. Its applications range from cancer diagnosis [32,33] to corneal tissue analysis [8,18], where an early and accurate diagnosis is critical.

Since corneal pathologies often modify the stromal collagen arrangement [8,12–14,18], any technique capable of detecting structural modifications prior to cornea deformation and/or opacification will be of special interest. The purpose of this study was to establish objective metrics based on SHG imaging to analyze collagen distribution, image quality and polarization sensitivity in human corneas. Both control and diseased corneas were characterized without using external labels. This allows for an optimized imaging protocol to be established for the analysis of tissues affected by collagen disorders.

The results reported in this study show that the collagen patterns visualized through SHG microscopy can be objectively classified by computing the SD parameter (Figure 3). In this sense, pathological tissues are related to higher SD values (i.e., collagen disorganization), which is in accordance with the previous literature [8,18].

In addition, our study also includes a quantitative analysis of the changes induced by temporal human edema progression (Figures 4 and 5). The corneal edematous process led to a loss of visibility of the collagen fibers (i.e., a noticeable decrease in fiber delineation), together with a progressive increase in SD values. This structural alteration is consistent with that reported by Hsueh et al. [31], although they did not present an analysis of the edema temporal evolution.

Studies on collagen changes as a function of time are of great interest to explore the temporal response of the tissue to pathologies, surgical procedures and external damages [9–11]. Quantitative assessment of temporal corneal recovery during natural healing is also useful to understand corneal recovery and collagen rearrangement [34].

In contrast, an exponential correlation between SD and objective SHG image quality metrics was also found (Figures 6 and 7). In particular, acutance and entropy behave similarly. This behavior indicates a rapid deterioration of the image resolution and the visualization of biological features as collagen alignment is modified. The usefulness of these metrics to explore and improve ocular imaging has been demonstrated in the past [29,35,36]. From a clinical point of view, the exponential dependence reported here is critical, as certain pathological stages might present high/medium SD values with hardly visible collagen structures (i.e., low image quality), which might lead to a non-accurate diagnosis. The choice of appropriate metrics might optimize and speed up the outputs of

deep-learning methods aimed at human cornea classification in terms of differentiating healthy and diseased samples.

Although SHG signal polarization sensitivity was discovered early on [19], polarimetric SHG imaging of human corneas is scarce, and only linear polarization has been employed [23,37,38]. These linear states were mainly used to better visualize collagen fibers and compute their orientation. However, to the best of our knowledge, studies on human cornea polarization sensitivity and the relationship with collagen distributions have not been reported previously.

Polarimetric SHG microscopy has gained popularity due to its potential to discriminate normal collagen tissues from pathological ones in skin dermis and lung tissues [39,40]. Its use with human corneas represents a step forward toward the characterization of different diseases with promising applications in clinical environments.

In the present experiment, for each human cornea involved, polarimetric SHG images corresponding to four independent states were acquired. This set of four images was used to compute the spatial resolved map of modulation. This parameter allowed a better understanding of the differences in SHG intensity as a function of the polarization state of the excitation light. The results show a statistically significant linear correlation between the SHG modulation map and SD (Figure 11). This behavior indicates that the less organized the human cornea is (i.e., more pathological), the lower the response to the incident polarization state. Consequently, SHG images of non-organized corneas present not only a low image quality (Figures 6 and 7) but also reduced polarization sensitivity.

In addition, when modulation is high (see, for instance, Figure 9), one of the four polarimetric SHG images might be chosen as the optimum one, which is associated with both an improved optical quality and a better visualization of morphological features. This fairly agrees with previous publications reporting a biological structural link between the orientation of collagen fibers and the maximum SHG intensity [28], which might also provide a methodology to select an optimal incident polarization to better characterize tissues [22]. As expected, this fact only occurs with organized and partially organized corneas, since non-organized corneas hardly reveal differences in SHG intensity among the four polarimetric images.

These results indicate that polarimetric SHG imaging used in this study presents a double experimental function: (1) it can be used as an alternative tool to obtain information on collagen structural distribution (which might avoid the use of the structure tensor or equivalent algorithms [8,15,17,18] as Figure 11 demonstrates), and (2) it allows one to acquire (when possible) an improved SHG image that provides a better visualization of biological features within the image (which might not appear when using other polarization states [26].

5. Conclusions

Polarimetric SHG microscopy was employed to obtain images from human corneas (healthy and pathological) presenting different collagen spatial arrangements. Collagen organization was quantified using the structure tensor method and, in particular, through the SD parameter.

Image quality was found to have an exponential dependence with the external corneal organization. This showed a rapid decrease in the accurate visualization of the stromal collagen fibers, which was associated with the morphological changes produced by certain pathological procedures.

The sensitivity to polarization of the SHG images was explored through so-called polarimetric modulation, defined as the contrast between the maximum and minimum SHG intensities for four independent polarization states. This modulation was linearly correlated to the SD values of the corneas, which indicates that corneal polarization sensitivity is strongly linked to the organization of stromal collagen fibers. The visualization of special details might be optimized and highlighted using certain polarization states, which might be of special importance in diseased corneas.

Lower modulation values are associated with a loss of organization within the spatial arrangement of collagen. This fact might be used to detect changes originating at the initial stages of the pathological processes, which could be useful for early detection.

The effects of some corneal diseases are not readily visible, and the patients are only aware of them at a later stage, when their visual function is significantly reduced. In that sense, quantitative assessments to distinguish between healthy and pathological corneas (at different stages) are highly recommended.

We have demonstrated the use of polarimetric SHG microscopy and image quality metrics to provide valuable descriptors of the human corneal structure. This opens a new door to the characterization of temporal evolution of human corneal disease. The usefulness of these approaches might have clinical applications given their potential for enabling fast and accurate objective procedures. This information can be used for corneal collagen characterization, early diagnosis or tracking of pathologies, as well as for a better understanding of their mechanisms of action. Future clinical applications for living human eyes [19] can reduce the subjective and time-consuming diagnosis process and can be used for automated screening.

Author Contributions: Conceptualization and experiment design, J.M.B. and I.Y.; experimental measurements, J.M.B. and R.M.M.-O.; data curation and analysis, R.M.M.-O. and F.J.Á.; writing, J.M.B.; review, R.M.M.-O., I.Y. and F.J.Á.; software development and testing, R.M.M.-O. and F.J.Á. All authors have read and agreed to the published version of the manuscript.

Funding: This research was partially supported by the Agencia Estatal de Investigación, Spain (grant PID2020-113919RB-I00).

Institutional Review Board Statement: The protocol of this study was approved by the Ethical Research Committee of both Universidad de Murcia and Hospital Universitario Virgen de la Arrixaca, Murcia (the latter regarding the privacy of data collected from completely anonymized donors).

Informed Consent Statement: Not applicable.

Data Availability Statement: Requests for materials should be addressed to J.M.B.

Acknowledgments: The authors thank Luis Ordóñez Angamarca, for helping during the early steps of the experiment.

Conflicts of Interest: The authors declare no conflict of interest.

References

1. Komai, Y.; Ushiki, T. The three-dimensional organization of collagen fibrils in the human cornea and sclera. *Invest. Ophthalmol. Vis. Sci.* **1991**, *32*, 2244–2258. [PubMed]
2. Yeh, A.T.; Nassif, N.; Zoumi, A.; Tromberg, B.J. Selective corneal imaging using combined second-harmonic generation and two-photon excited fluorescence. *Opt. Lett.* **2002**, *27*, 2082–2084. [CrossRef] [PubMed]
3. Morishige, N.; Petroll, W.M.; Nishida, T.; Kenney, M.C.; Jester, J.V. Noninvasive corneal stromal collagen imaging using two-photon-generated second-harmonic signals. *J. Cataract. Refract. Surg.* **2006**, *32*, 1784–1791. [CrossRef] [PubMed]
4. Aptel, F.; Olivier, N.; Deniset-Besseau, A.; Legeais, J.-M.; Plamann, K.; Schanne-Klein, M.-C.; Beaurepaire, E. Multimodal nonlinear imaging of the human cornea. *Invest. Ophthalmol. Vis. Sci.* **2010**, *51*, 2459–2465. [CrossRef]
5. Bueno, J.M.; Gualda, E.J.; Artal, P. Analysis of corneal stroma organization with wavefront optimized nonlinear microscopy. *Cornea* **2011**, *30*, 692–701. [CrossRef]
6. Maurice, D.M. The structure and transparency of the cornea. *J. Physiol.* **1957**, *136*, 263–286. [CrossRef]
7. Meek, K.M.; Knupp, C. Corneal structure and transparency. *Prog. Retin. Eye Res.* **2015**, *49*, 1–16. [CrossRef]
8. Batista, A.; Breunig, H.G.; König, A.; Schindele, A.; Hager, T.; Seitz, B.; König, K. High-resolution, label-free two-photon imaging of diseased human corneas. *J. Biomed. Opt.* **2018**, *23*, 036002. [CrossRef]
9. Bueno, J.M.; Ávila, F.J.; Martínez-García, M.C. Quantitative analysis of the corneal collagen distribution after in vivo cross-linking with second harmonic microscopy. *BioMed Res. Int.* **2019**, *2019*, 3860498. [CrossRef]
10. Matteini, P.; Ratto, F.; Rossi, F.; Stringari, C.; Kapsokalyvas, D.; Pavone, F.S.; Pini, R. Photothermally-induced disordered patterns of corneal collagen revealed by SHG imaging. *Opt. Express* **2009**, *17*, 4868–4878. [CrossRef]
11. Wu, Q.; Yeh, A.T. Rabbit cornea microstructure response to changes in intraocular pressure visualized by using nonlinear optical microscopy. *Cornea* **2008**, *27*, 202–208. [CrossRef] [PubMed]

12. Tan, H.Y.; Sun, Y.; Lo, W.; Lin, S.J.; Hsiao, C.H.; Chen, Y.F.; Huang, S.C.; Lin, W.C.; Jee, S.H.; Yu, H.S.; et al. Multiphoton fluorescence and second harmonic generation imaging of the structural alterations keratoconus ex vivo. *Invest. Ophthalmol. Visual Sci.* **2006**, *47*, 5251–5259.
13. Tan, H.-Y.; Sun, Y.; Lo, W.; Teng, S.W.; Wu, R.J.; Jee, S.H.; Lin, W.C.; Hsiao, C.H.; Lin, H.C.; Chen, Y.F.; et al. Multiphoton fluorescence and second harmonic generation microscopy for imaging infectious keratitis. *J. Biomed. Opt.* **2007**, *12*, 24013. [CrossRef] [PubMed]
14. Morishige, N.; Yamada, N.; Zhang, X.; Morita, Y.; Yamada, N.; Kimura, K.; Takahara, A.; Sonoda, K.-H. Abnormalities of stromal structure in the bullous keratopathy cornea identified by second harmonic generation imaging microscopy. *Invest. Ophthalmol. Vis. Sci.* **2012**, *53*, 4998–5003. [CrossRef] [PubMed]
15. Lombardo, M.; Serrao, S.; Barbaro, V.; Di Iorio, E.; Lombardo, G. Multimodal imaging quality control of epithelia regenerated with cultured human donor corneal limbal epithelial stem cells. *Sci. Rep.* **2017**, *7*, 515401–515410.
16. Batista, A.; Breunig, H.G.; König, A.; Schindele, A.; Hager, T.; Seitz, B.; Morgado, A.M.; König, K. Assessment of human corneas prior to transplantation using high-resolution two-photon imaging. *Invest. Ophthalmol. Vis. Sci.* **2018**, *59*, 176–184. [CrossRef] [PubMed]
17. Batista, A.; Breunig, H.G.; Hager, T.; Seitz, B.; König, K. Early evaluation of corneal collagen crosslinking in ex-vivo human corneas using two-photon imaging. *Sci. Rep.* **2019**, *9*, 10241. [CrossRef]
18. Ávila, F.J.; Artal, P.; Bueno, J.M. Quantitative discrimination of healthy and diseased corneas with second harmonic generation microscopy. *Trans. Vis. Sci. Tech.* **2019**, *83*, 51. [CrossRef]
19. Ávila, F.J.; Gambín, A.; Artal, P.; Bueno, J.M. In vivo two-photon microscopy of the human eye. *Sci. Rep.* **2019**, *9*, 10121. [CrossRef]
20. Roth, S.; Freund, I. Second harmonic generation in collagen. *J. Chem. Phys.* **1979**, *70*, 1637–1643. [CrossRef]
21. Brasselet, S. Polarization-resolved nonlinear microscopy: Application to structural molecular and biological imaging. *Adv. Opt. Photon.* **2011**, *3*, 205–271. [CrossRef]
22. Hristu, R.; Stanciu, S.G.; Tranca, D.E.; Stanciu, G.A. Improved quantification of collagen anisotropy with polarization-resolved second harmonic generation microscopy. *J. Biophotonics* **2017**, *10*, 1171–1179. [CrossRef] [PubMed]
23. Latour, G.; Gusachenko, I.; Kowalczuk, L.; Lamarre, I.; Schanne-Klein, M.C. In vivo structural imaging of the cornea by polarization-resolved second harmonic microscopy. *Biomed. Opt. Express* **2012**, *3*, 1–15. [CrossRef]
24. Ávila, F.J.; del Barco, O.; Bueno, J.M. Polarization dependence of aligned collagen tissues imaged with second harmonic generation microscopy. *J. Biomed. Opt.* **2015**, *20*, 86001. [CrossRef] [PubMed]
25. Ávila, F.J.; del Barco, O.; Bueno, J.M. Polarization response of second-harmonic images for different collagen spatial distributions. *J. Biomed. Opt.* **2016**, *21*, 66015. [CrossRef]
26. Stefan, G.; Stanciu, S.G.; Ávila, F.J.; Hristu, R.; Bueno, J.M. A Study on image quality in polarization-resolved second harmonic generation microscopy. *Sci. Rep.* **2017**, *7*, 15476.
27. Ávila, F.J.; Bueno, J.M. Analysis and quantification of collagen organization with the structure tensor in second harmonic microscopy images of ocular tissues. *Appl. Opt.* **2015**, *54*, 9848–9854. [CrossRef]
28. Ávila, F.J.; del Barco, O.; Bueno, J.M. Quantifying external and internal collagen organization from Stokes-vector-based second harmonic generation imaging polarimetry. *J. Opt.* **2017**, *19*, 105301. [CrossRef]
29. Hunter, J.J.; Cookson, C.J.; Kisilak, M.L.; Bueno, J.M.; Campbell, M.C.W. Characterizing image quality in a scanning laser ophthalmoscope with differing pinholes and induced scattered light. *J. Opt. Soc. Am. A* **2007**, *24*, 1284–1295. [CrossRef]
30. Bueno, J.M.; Skorsetz, M.; Bonora, S.; Artal, P. Wavefront correction in two-photon microscopy with a multi-actuator adaptive lens. *Opt. Express* **2018**, *26*, 14278–14287. [CrossRef]
31. Hsueh, C.M.; Lo, W.; Chen, W.L.; Hovhannisyan, V.A.; Liu, G.Y.; Wang, S.S.; Tan, H.Y.; Dong, C.Y. Structural characterization of edematous corneas by forward and backward second harmonic generation imaging. *Biophys. J.* **2009**, *97*, 1198–1205. [CrossRef] [PubMed]
32. Keikhosravi, A.; Bredfeldt, T.S.; Sagar, A.K.; Eliceiri, K.W. Second-harmonic generation imaging of cancer. *Methods Cell Biol.* **2014**, *123*, 531–546. [PubMed]
33. Bueno, J.M.; Ávila, F.J.; Hristu, R.; Stanciu, S.G.; Eftimie, L.; Stanciu, G.A. Objective analysis of collagen organization in thyroid nodule capsules using second harmonic generation microscopy images and the Hough transform. *Appl. Opt.* **2020**, *59*, 6925–6931. [CrossRef] [PubMed]
34. Bueno, J.M.; Ávila, F.J.; Lorenzo-Martín, E.; Gallego-Muñoz, P.; Martínez-García, M.C. Assessment of the corneal collagen organization after chemical burn using second harmonic generation microscopy. *Biomed. Opt. Express* **2021**, *12*, 756. [CrossRef]
35. Choong, Y.F.; Rakebrandt, F.; North, R.V.; Morgan, J.E. Acutance, an objective measure of retinal nerve fibre image clarity. *Br. J. Ophthamol.* **2003**, *87*, 322–326. [CrossRef]
36. Martínez-Ojeda, R.M.; Hernández-García, C.; Bueno, J.M. Enhancement of second harmonic microscopy images in collagen-based thick samples using radially polarized laser beams. *Opt. Commun.* **2021**, *499*, 127273. [CrossRef]
37. Alizadeh, M.; Merino, D.; Lombardo, G.; Lombardo, M.; Mencucci, R.; Ghotbi, M.; Loza-Alvarez, P. Identifying crossing collagen fibers in human corneal tissues using pSHG images. *Biomed. Opt. Express* **2019**, *10*, 3875–3888. [CrossRef]
38. Mercatelli, R.; Mattana, S.; Capozzoli, L.; Ratto, F.; Rossi, F.; Pini, R.; Fioretto, D.; Pavone, F.S.; Caponi, S.; Cicchi, R. Morpho-mechanics of human collagen superstructures revealed by all-optical correlative micro-spectroscopies. *Commun. Biol.* **2019**, *2*, 117. [CrossRef]

39. Su, P.J.; Chen, W.L.; Hong, J.B.; Li, T.H.; Wu, R.J.; Chou, C.K.; Chen, S.J.; Hu, C.; Lin, S.J.; Dong, C.Y. Discrimination of collagen in normal and pathological skin dermis through second-order susceptibility microscopy. *Opt. Express* **2009**, *17*, 11161–11171.
40. Golaraei, A.; Cisek, R.; Krouglov, S.; Navab, R.; Niu, C.; Sakashita, S.; Yasufuku, K.; Tsao, M.S.; Wilson, B.C.; Barzda, V. Characterization of collagen in non-small cell lung carcinoma with second harmonic polarization microscopy. *Biomed. Opt. Express* **2014**, *5*, 3562–3567. [CrossRef]